Refurbishing Inconel 738 blades in GE-Frame5 gas turbines through laser cladding and welding

Peyman Toosi[a], Hamid Zarepour[a]*, Mohammad-Ali Rezaei [b]

[a] Modern Manufacturing Technologies Research Center, Department of Mechanical Engineering, Najafabad Branch, Islamic Azad University, Najafabad, Iran

[b] Department of Materials Engineering, Tarbiat Modares University, Tehran, Iran

*Corresponding Author Email: h-zare@iaun.ac.ir

Abstract

This study investigates the refurbishment of first-stage Inconel 738 blades for GE-Frame 5 gas turbines using laser cladding and welding techniques. Laser welding was performed with a pulsed Nd:YAG system equipped with a manual 0.7 mm Inconel 625 filler wire feed. In contrast, laser cladding utilized a continuous fiber laser paired with an automated powder injection system for Inconel 625. Process parameters, including scanning speed, laser power output, and powder feeding rate, were optimized to enhance the laser cladding. Testing showed that laser settings of 400 W power, 15 g/s powder feed, and 8 mm/s scanning speed produced coatings with superior geometry, completely eliminated hot cracking, and minimized porosity. Preliminary weld tests identified optimal settings of 4 mm/s scanning speed at 5 kW maximum power. Subsequently, 20 layers were deposited to simulate worn blade tip repair welds. Both methods effectively reduced heat-affected zones through refined parameters. Pulsed laser welding with filler material broadened repair options for gas turbine blades. However, the surface hardness in treated areas was somewhat lower than that of the base material due to phase transformations occurring during laser cladding and welding.

Keywords: Laser welding, Laser cladding, Turbine blade refurbishment, Inconel 738

1. Introduction

Gas turbines are widely used rotary machines across various industrial sectors, including power plants, refineries, and aircraft engines [1,2]. To operate effectively under the challenging conditions of high temperatures, significant stresses, and corrosive environments, these machines require materials with exceptional characteristics. Nickel-based superalloys have emerged as an ideal solution due to their outstanding properties, including high tensile strength, creep strength, impact resistance, and corrosion resistance at both ambient and elevated temperatures [2,3]. Solid solution and precipitation-hardenable nickel-based superalloys comprise the hot sections of gas turbines. Inconel 738 is a prime example, renowned for its resilience derived from Ni3(Al, Ti) precipitates and MC carbides [4]. One of the primary causes of damage to turbine blades is tip wear, which results from thermal expansion during high-speed rotation and elevated temperatures, primarily due to contact with stator liners [5].
In gas turbines, the use of new repair technologies is often preferred over replacement in the hot sections due to lower costs. Traditional repair techniques such as plasma spraying [6],

Tungsten Inert Gas (TIG) welding [7], and plasma transferred arc welding [8], have been extensively studied. However, γ' precipitation in nickel-based superalloys with high Ti/Al content makes them susceptible to solidification cracking in the weld metal and liquation cracking in the heat-affected zone (HAZ) of repaired components [4].

Studies by Banerjee et al. show that the use of filler alloys with slow aging responses, smaller lattice mismatches between precipitating phases and matrix, lower concentrations of Ti/Al, and softer weld metals can reduce heat-affected zone cracking susceptibility of IN738LC welds [9]. Based on microstructural properties, micro-TIG welding appears superior to TIG welding when repairing turbine components fabricated from Inconel 738 and other precipitation-strengthened alloys. Varying capacitance, voltage, and current in the micro TIG welding of alloys IN625, IN718, and IN722 significantly affects void content and crack density [10].

The utilization of high-energy-density processes, such as laser welding, is a promising approach for repairing nickel-based superalloys. By reducing the heat input, this technique offers the opportunity to produce a welded part with a narrow heat-affected zone and without porosity and cracks while ensuring good metallurgical bonding [11].

During autogenous laser welding of Inconel 738, the melting of γ' precipitates and MC carbides causes a reduction in the melting temperature of grain boundaries, leading to the formation of large-sized HAZ liquation cracks. HAZ cracks primarily initiate from the base metal and extend towards the melting zone, predominantly propagating along solidification grain boundaries [12]. However, the use of filler metal (powder or wire) significantly mitigates HAZ cracking in this alloy. Harder fillers exhibit a higher occurrence of HAZ cracks whereas softer fillers experience a decrease in both size and length of such cracks [13].

Laser-based metal deposition technologies have been investigated for repairing gas turbine components, and these methods have exhibited suitable capabilities of meeting the necessary repair requirements. The laser deposition process involves the simultaneous melting of a thin layer of filler material by the laser beam, leading to a metallurgically-bonded mixture of melted filler and base material. In a study by Bielenin et al., the optimal position of Inconel 625 wire relative to the Nd:YAG laser beam was evaluated [14]. The researchers also determined that continuous physical contact between the wire and weld pool effectively prevented the formation of inhomogeneous droplets.

The study conducted by Brandt et al. has demonstrated that the direct laser deposition process provides superior speed and precision in repairing turbine blades in comparison to conventional procedures [15]. The process is influenced by multiple factors, including powder feeding rate, welding speed, focusing unit, and cladding nozzle.

Chen et al. introduced a laser cladding strategy utilizing surface build-up and 3D laser metal forming for restoring damaged IN738 blades [16]. The research findings indicate that the IN738 clad region possesses properties suitable for high-stress environments after applying an appropriate post-weld heat treatment, and exhibits superior characteristics compared to the IN625 clad region.

Given the studies mentioned above, the objective of this paper is to develop a low-heat-input method that employs laser technology to enhance the acceptance limit for repair welding of hot gas turbine components, particularly moving parts. Additionally, we aim to investigate two

techniques: laser welding with wire filler metal and laser cladding with powder filler metal, to evaluate their effectiveness in improving the surface properties of refurbished components.

2. Experimental Procedure

Inconel 738 turbine blades, as shown in **Fig. 1a,** were used as the test material. The blades were cut into samples measuring approximately 10 cm x 3 cm using a wire-cut machine. The specimens underwent heat treatment, which involved two hours of solution annealing at 1120°C, followed by air cooling. Subsequently, the blades were aged for sixteen hours at 845°C. **Table 1** presents the chemical composition of Inconel 738.

The restoration process was performed using laser welding, where coupons were joined using a Nd:YAG pulsed laser machine rated at 10 KW peak power. This equipment features both an XYZ table and a CCD camera to monitor the weld pool. Parameterization began with bead-on-plate laser welding. Subsequently, four welding lines, each 5 mm in length, were created using Inconel 625 filler with a diameter of 0.7 mm (**Fig. 1b**).

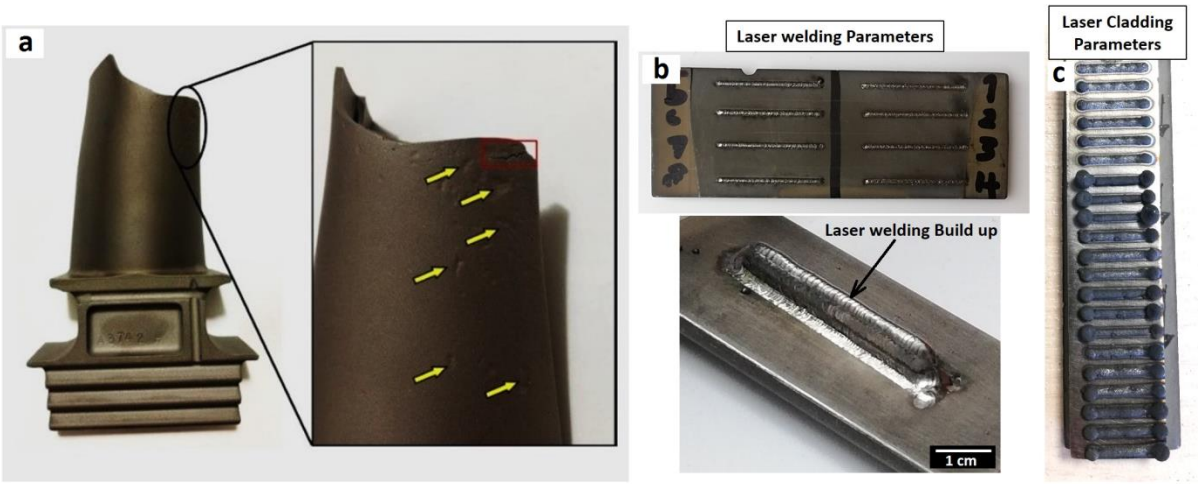

Fig. 1a Well-worn turbine blade along with surface cracks on its edge, **b** laser welding of specimens, **c** laser cladding of specimens

Table 1 Chemical composition of the IN-738 turbine blade and powder used

Alloy type	Elements (wt%.)											
	Ni	Cr	Co	Mo	Nb	Al	Ti	Ta	W	Mn	C	Fe
IN 738	62.40	16.40	9.04	1.64	0.74	3.63	3.24	1.70	2.48	0.02	0.08	0.17
IN 625	62.20	21.20	0.80	9.20	3.80	-	0.40	-	-	0.18	0.05	0.80

Laser welding parameters are outlined in **Table 2**. It is crucial to ensure that the laser beam does not make full contact with either the workpiece or the filler during welding. Therefore, it is recommended that 70% of the beam focus on the filler, while the remaining 30% is directed towards the workpiece. Additionally, the optimal angle of incidence for the beam when reaching the workpiece is set at 45°. This was determined based on a series of preliminary pilot tests and the experience gained by the laser system operator. To simulate the actual conditions of turbine blade repair, 20 layers were built up while selecting only one parameter set.

A YFL-500 continuous wave fiber laser source, with a maximum output power of 500 watts, was used to conduct laser cladding tests. The laser beam had a wavelength of 1080 nm, an optical efficiency of 78%, a focal distance of 100 mm, and beam quality close to unity. This equipment featured a twin powder spraying system with coaxial powder head and nozzles, integrated within a 5-axis CNC system. Laser scanning speed (mm/s), power (W), and powder feeding rate (g/s) were three variables used to optimize the parameters for the laser cladding. A combination of three scanning speeds (6, 8, and 10 mm/s), three laser powers (200, 300, and 400 W), and three powder feeding rates (10, 15, and 20 g/s) were selected in order to determine the appropriate parameters. **Fig. 1c** depicts the laser-cladded samples while **Table 3** presents the relevant laser cladding parameters, selected based on a number of preliminary trial tests.

A perpendicular section was obtained from the welded specimens using an electric discharge machine (EDM). The welded specimens were then mounted, polished, and etched with a solution containing 10 g of $CuSO_4$, 50 ml of H_2O, and 50 ml of HCl (10g). Microstructural characterization of the samples was conducted using an Olympus BX51 M optical microscope (OM) and a Tescan Corporation Mira3 model field emission scanning electron microscope (FESEM) equipped with an energy dispersive spectrometer (EDS).

Table 2 Laser welding parameters

Sample Abbreviations	Peak Power (KW)	Average Power (W)	Pulse Duration (ms)	Pulse Frequency (Hz)	Welding Speed (mm/s)	Heat Input (J/mm)	Pulse Shape
W1	2.7	193	16	6	4	96.5	Annealing
W2	2.7	193			2	48.2	
W3	5	275			2	137.5	
W4	5	275			4	68.7	

Table 3 Laser cladding parameters

Sample Abbreviations	Power (W)	Scanning Speed (mm/s)	Powder Feeding Rate (g/s)	Dilution (%)	Heat Input (J/mm)
C1	200	6	15	0	33.3
C2	300	6	15	12.7	50
C3	400	6	15	24.1	66.6
C4	400	8	10	25.8	50
C5	400	8	15	22.9	50

C6	400	8	20	14.5	50
C7	400	6	20	5.6	66.6
C8	400	8	20	14.5	50
C9	400	10	20	20.2	40

3. Results and Discussion

3.1. Microstructural investigation of the base metal

The microstructure of Inconel 738 superalloy consists of austenitic equiaxed grains, gamma prime precipitate, and MC carbides, which can exist in both cubic and non-cubic forms, significantly enhancing its high-temperature strength. Fig. 2 displays cubic, non-cubic, and elongated MC carbides found in Inconel 738. The metallic constituents of MC carbide include titanium (Ti), tantalum (Ta), niobium (Nb), and chromium (Cr). Energy-dispersive X-ray spectroscopy (EDS) analysis of scanning electron microscope (SEM) images reveals that Ti is predominantly present in cubic MC carbides, while elongated, non-cubic MC carbides contain significant amounts of Ta or Nb.

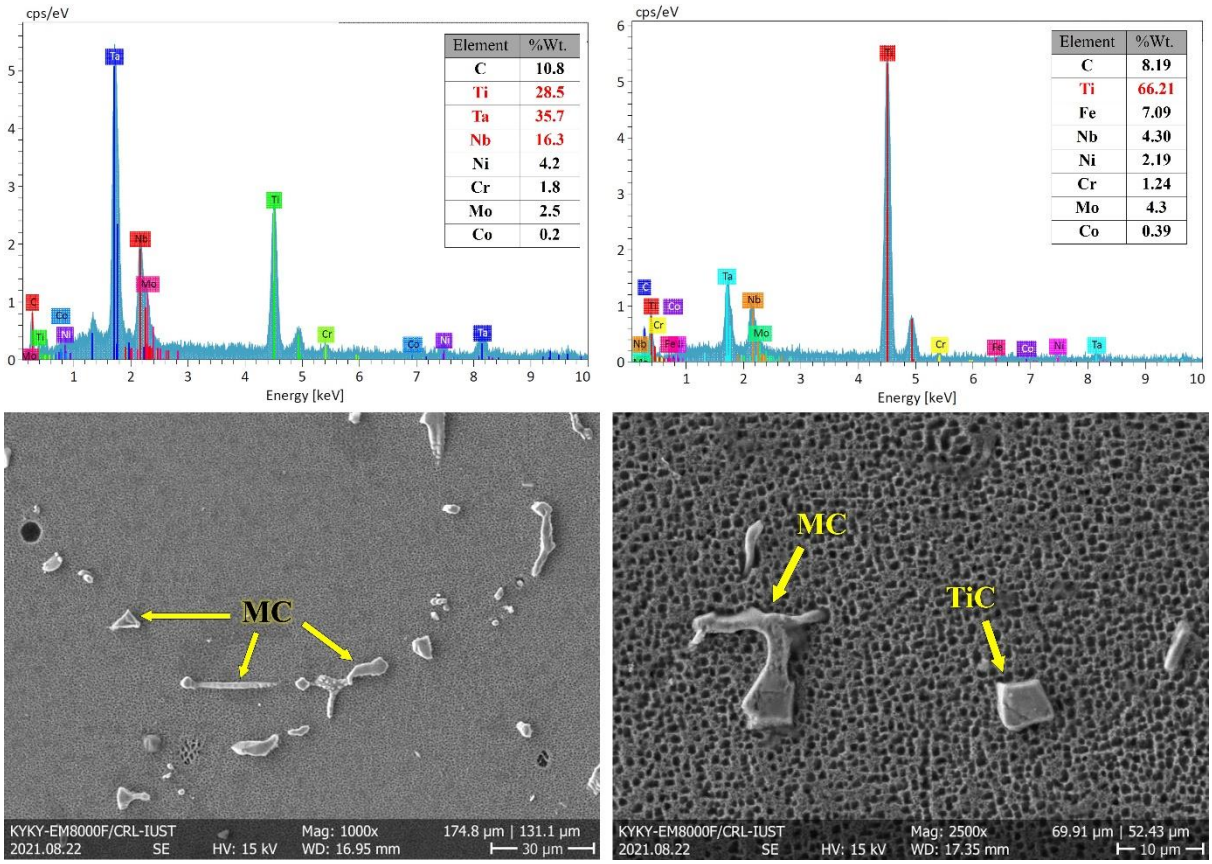

Fig. 2 Ti-rich cubic MC carbides and Ta, Nb and Ti-rich non-cubic MC carbides

3.2. Geometrical investigation of deposited layer

Fig. 3 illustrates the Inconel 625 filler metal deposited through laser welding, showing suitable weld pools and build-up layers. Among all the samples, only sample W3 exhibited porosity in

the weld pool depth, while the other samples showed no solidification or liquation cracks, gas porosity, or failure to fuse with the filler metal. The favorable depth-to-width ratio of the weld pool and deposited layer was achieved with only two welding passes, along with acceptable adhesion to the substrate. Additionally, the pulsed nature of the laser produced distinct solidification lines in each layer.

The results indicate that the increasing laser power, laser beam density, and heat input are associated with higher dilution percentages. A decrease in laser power results in less energy entering the substrate, which causes more energy to be expended on melting the filler in the build-up area, ultimately leading to a smaller width of the build-up area. A study by Taheri et al. also reported similar findings in the laser welding of the superalloy GTD-111 [17].

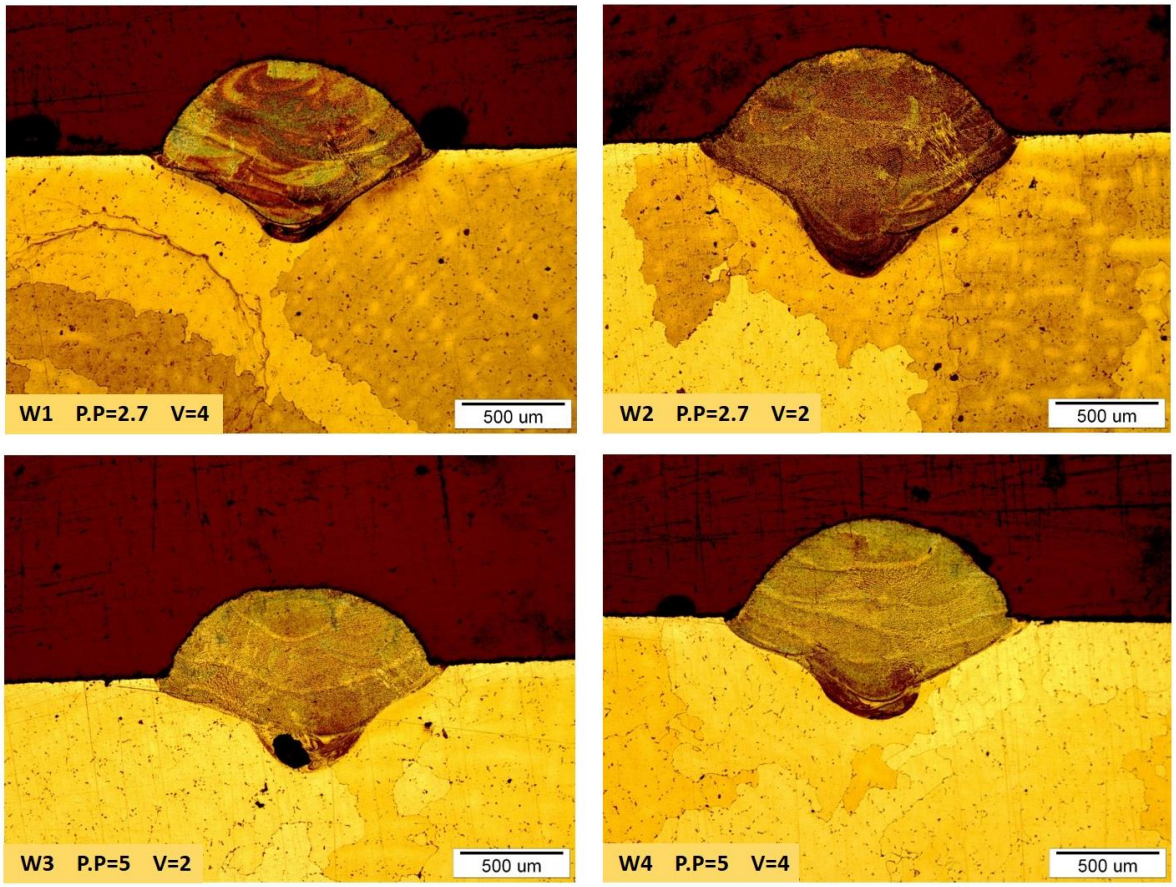

Fig. 3 Optical macrographs of cross sections of W1 to W4 build-up in laser welding

Fig. 4 portrays a comparison between the geometries of single-pass laser cladding with different parameters. Maintaining a constant scanning speed and powder feeding rate, an increase in laser power is noted in samples C1 to C3. Optical microscope (OM) images revealed inadequate melting of powder particles at 200 watts of power, resulting in a narrow cladded area with no dilution. However, an increase in laser power led to an increase in dilution percentage, although sample C7 displayed a superior cladding geometry.
Regarding samples C4 to C6, it was observed that increasing the powder feeding rate while keeping laser power and welding speed constant led to a reduction in dilution percentage.

However, the resulting cladding geometry was less desirable. A higher powder feeding rate reduces the heat input, whereas raising the scanning speed decreases the powder availability per unit length of the cladding [13]. Due to the width-to-height ratio, a large portion of the substrate melts in the molten pool which increases dilution significantly. Consequently, it can be affirmed that by increasing the powder feeding rate in samples equivalent to lower heat input, the dilution percentage may decrease. The optimized result was displayed in sample C4. Lastly, when laser power and powder feeding rate were kept constant, and the scanning speed was increased in samples C7 to C9, incomplete melting of powder particles became more evident on the outer surface of the clad layer. The situation worsened, as an increase in scanning speed led to more holes and porosity. Multiple passes, with high overlap, may reduce the effect of these partially melted particles.

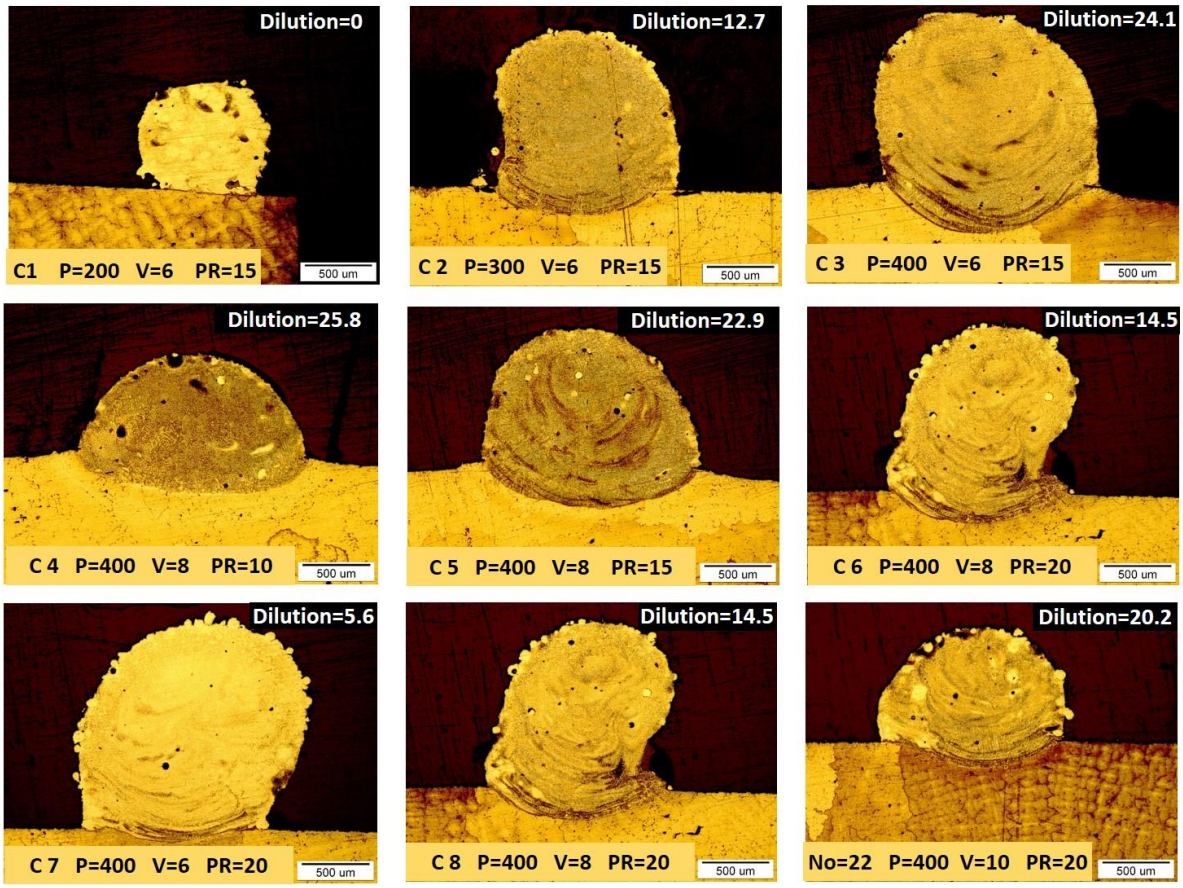

Fig. 4 Optical macrographs of cross sections of C1 to C9 build-up in laser cladding

3.3. Microstructural characterization of deposited layer

Fig. 5 presents a higher magnification view of the morphology of the laser build-up region of sample W1. The shape of grains within the deposited area is influenced by the solidification mode (G/R), while their size is determined by the cooling rate (G×R) [18]. A high thermal gradient at the interface between the weld metal and the substrate promotes planar growth. However, as the distance from the interface increases and the G/R ratio decreases, the level of undercooling rises, leading to the development of cellular microstructures that transition into

dendritic forms. This progression occurs from the edges of the weld towards its center, where the dendrites gradually evolve from the cellular to coaxial structures.

The laser process achieves a faster solidification rate compared to techniques such as plasma transferred arc (PTA) and tungsten inert gas (TIG) welding, resulting in finer microstructures [6, 19]. When repairing and reconstructing Inconel 738 using fusion welding methods like gas tungsten arc welding (GTAW) or laser welding, the melting temperature of grain boundaries is reduced, leading to rapid heating and melting of these zones during subsequent welding passes [20]. Additionally, localized heating through high-energy-density methods, such as laser or electron beam welding, enhances the mechanical properties of the welds by creating a smaller heat-affected zone (HAZ) and fine microstructures [21,22]. This reduced HAZ minimizes the influence of grain boundaries on crack initiation and growth. The Inconel 625 filler metal is capable of withstanding higher temperatures during the solidification of Inconel 738 while effectively absorbing contraction stresses, thereby preventing hot cracking. Consequently, Nd:YAG pulsed laser welding combined with a filler metal can expand the acceptance limit for repair welding.

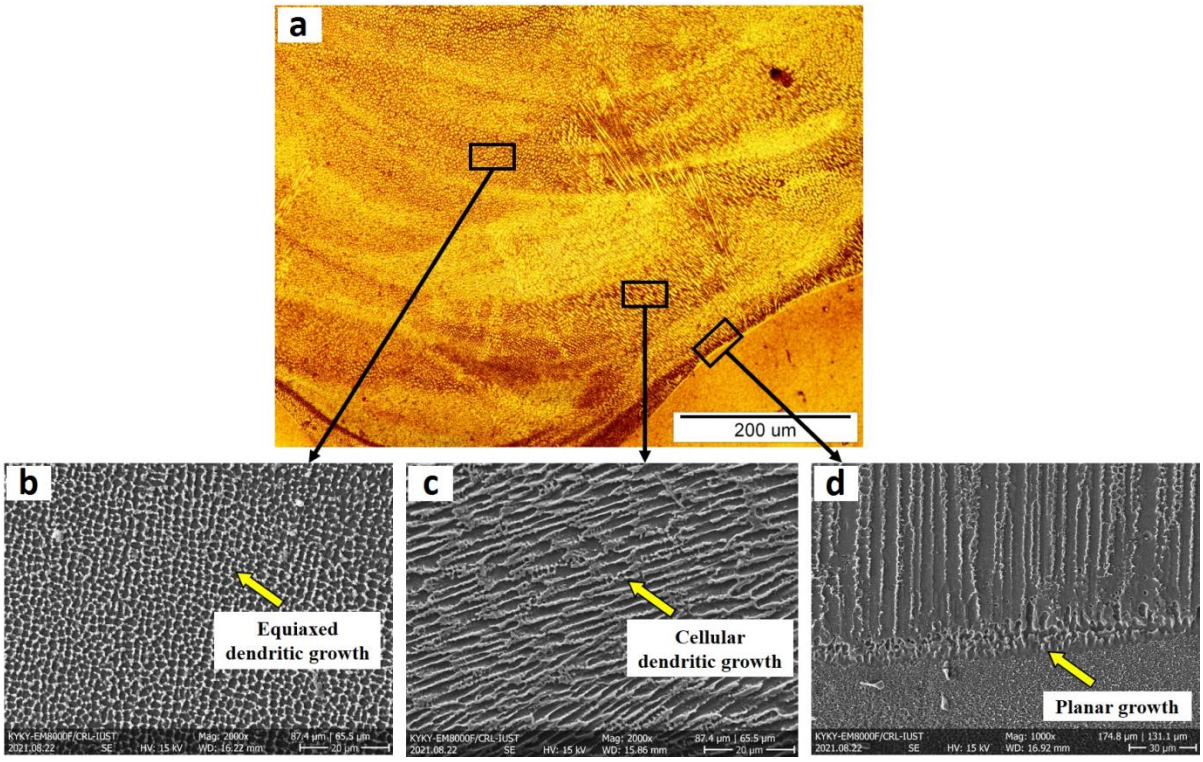

Fig. 5a Morphology of the deposited welded metal of sample W1, **b** equiaxed dendritic growth in center of the weld metal, **c** cellular dendritic growth, **d** planar growth in WM/HAZ interface

Fig. 6 illustrates the deposition of 20-layer laser-welded sample, which displays favorable surface adhesion of the built-up area onto the base metal, while being devoid of any cracks or porosity. The Marangoni lines are also visible in the weld pool between the build-up area and base metal due to the nature of pulsating laser deposition with filler.

The fluid flow within the molten pool formed during laser welding or laser additive manufacturing is influenced by four primary forces: buoyancy force arising from liquid metal density, Marangoni force, which results from surface tension gradients, gravity, and shear forces caused by vapor or laser-induced plasma [23]. Additionally, recoil pressure serves as the primary driving force for molten metal during keyhole welding.

In the laser molten pool, the dominant mechanism is the gradient, with Marangoni forces generating shear stress that induces convection flow. As the laser moves, the highest temperature at the center of the molten pool decreases radially, creating a difference in surface tension that leads to an outward flow of molten metal. A reduction in laser welding speed significantly increases the interaction time between the laser and the surface, as well as the peak temperature. Consequently, this results in a steeper temperature gradient, which enhances Marangoni fluid convection and enlarges the melt pool. This phenomenon is evident in the higher magnification shown in **Fig. 6**. Furthermore, the ratio of weld to base metal (WM/BM) interfaces displays unmelted carbides due to the low heat input from the laser.

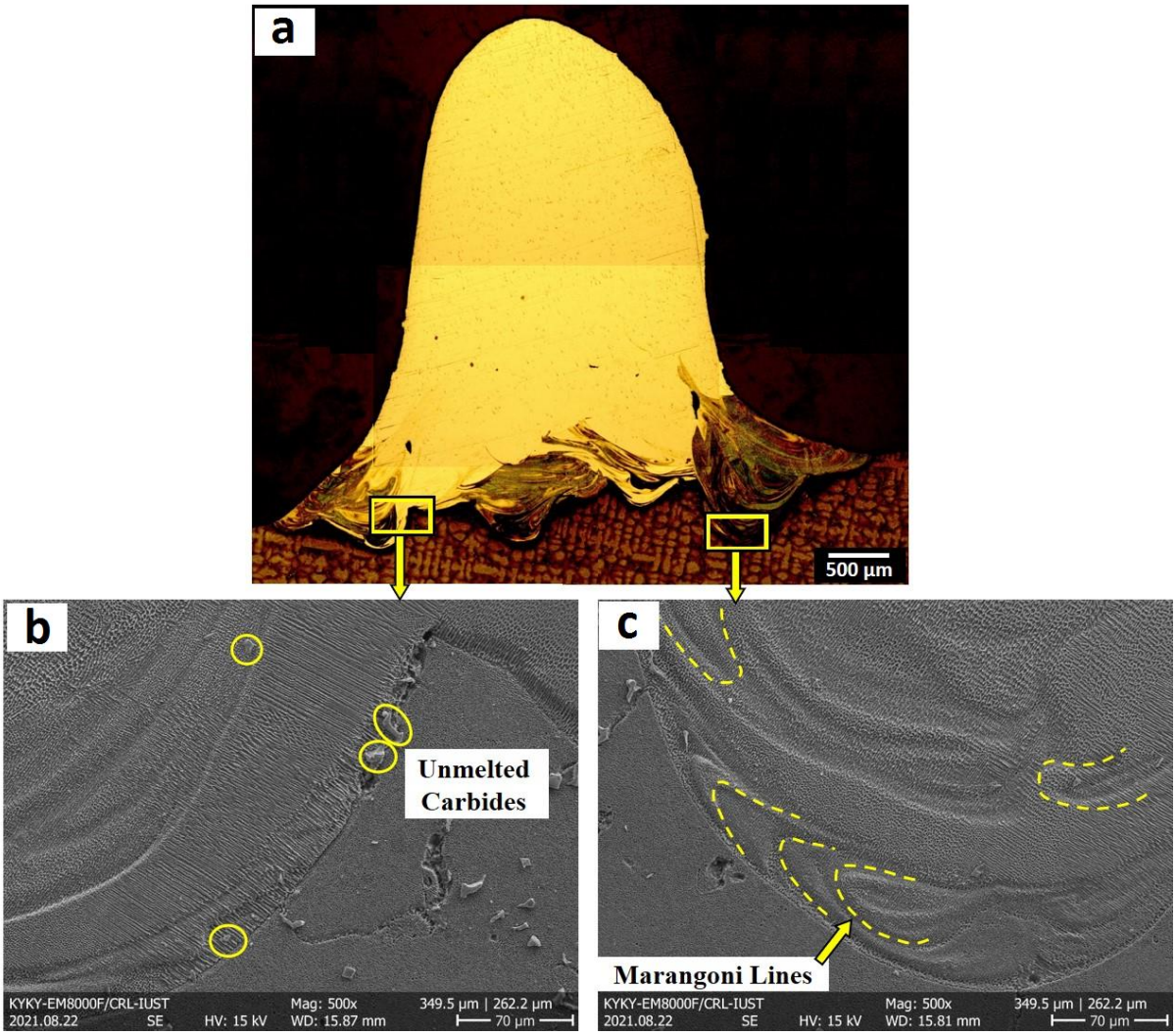

Fig. 6a 20-layer laser weld deposited sample, **b** unmelted carbides in WM/HAZ interface, **c** marangoni lines of the molten pool

The solidification process of Ni-base alloys leads to the enrichment of the interdendritic regions with alloying elements that possess an equilibrium distribution coefficient (k) less than unity (k < 1). In laser welding, the cooling rate determines the final distribution of secondary phases among dendritic structures, which consequently results in the formation of a fine microstructure. As depicted in **Fig. 7**, laser cladding produced weld metal with fine dendritic structure showcasing dark cores after etching and bright interdendritic regions. Additionally, the weld metal exhibited small particles of the second phase located within interdendritic regions and dendrite cores. The resolidified products had columnar dendrites, with noticeable segregation of niobium.

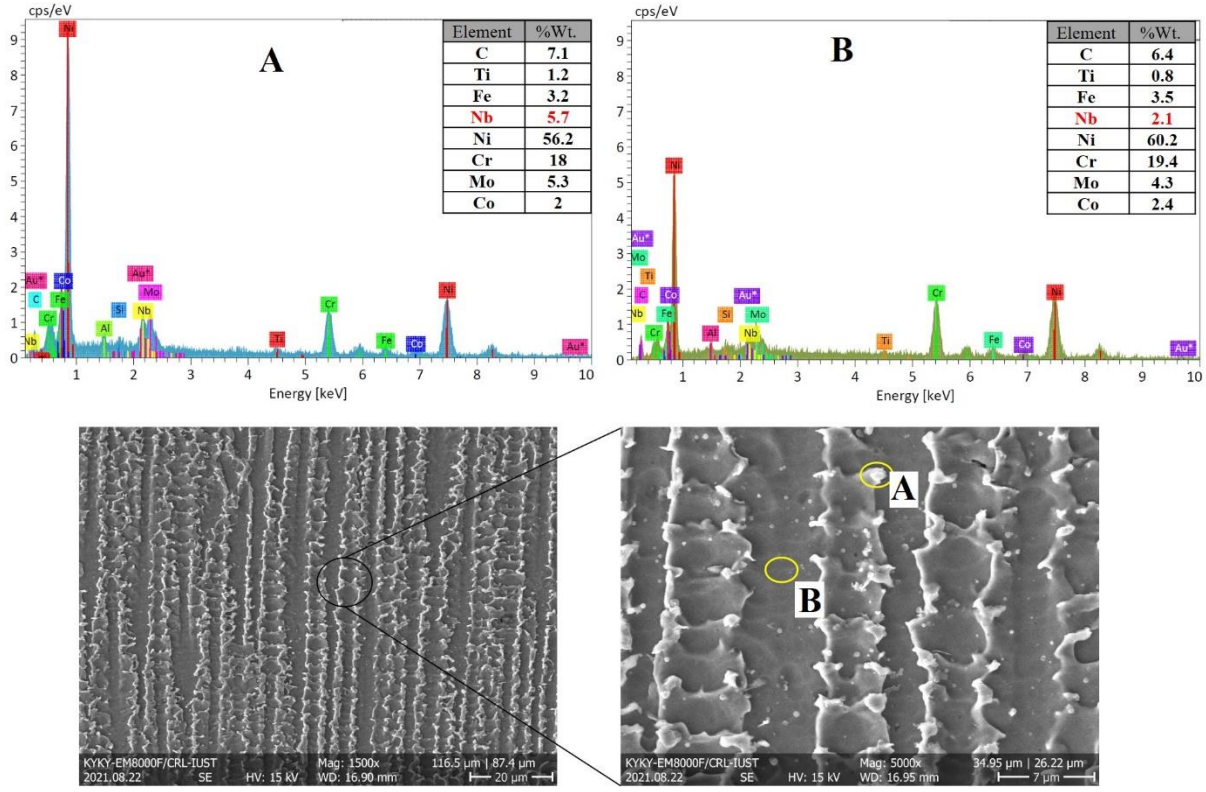

Fig. 7 Fine columnar dendrite in weld metal with bright etching interdendritic regions and dark etching core in higher magnification; niobium segregation indicated by A and B symbols

3.4 Microhardness test

In Fig. 8, the microhardness test results are presented for three regions of the samples, namely, the heat-affected zone (HAZ), dilution area, and cladding area. While the cladding area in samples C3, C6, and C9 has an average microhardness of 330, 336, and 359 Vickers, respectively, the average microhardness of the base metal measured is 372 Vickers. In general, the lower microhardness value of the cladding area indicates the dissolution of strengthening precipitates present in the base metal, such as TiC, TaC, and γ' during the laser cladding process. Interestingly, the cladded area exhibited slightly higher microhardness values in sample C9 as compared to sample C3. This could be attributed to the formation of smaller dendrites in the cladded areas due to the thermal gradient and the higher cooling rate, which can contribute to higher microhardness. However, it is important to note that the microhardness

of all investigated samples in the heat-affected zones was lower than that of the base metal due to critical thermal effects. It is essential to acknowledge that the heat-affected zones encountered temperatures reaching approximately 1000°C within a fraction of a second, causing a reduction in microhardness.

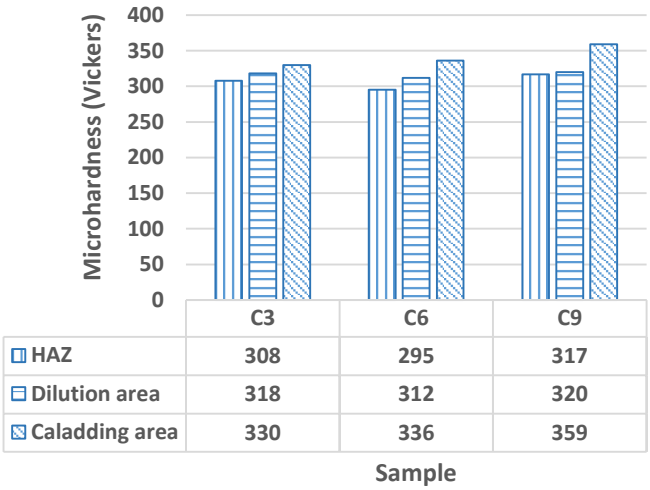

Fig. 8 Average microhardness (Vickers) of different areas in laser cladding process

4. Conclusions

1. Laser deposition process on Inconel 738 turbine blade specimens was performed successfully, using laser welding with Inconel 625 filler and laser cladding with Inconel 625 powder.
2. Hot cracks were observed in laser-welded specimens with no filler, but no cracks were observed in laser-welded specimens using Inconel 625 filler as well as laser-cladded specimens using Inconel 625 powder.
3. The optimal parameters for the laser cladding process were identified as a power of 400 W, a powder feeding rate of 15 g/s, and a welding speed of 8 mm/s, as these settings resulted in appropriate geometric shapes and reduced porosity compared to other samples.
4. The heat-affected zone was reduced, and proper geometric shape of the reconstructed area was achieved, resulting in increased acceptance limit in repair welding of moving turbine blades using pulsed laser welding with filler.
5. The use of Inconel 625 as a filler material, in both powder and wire forms, effectively withstands higher temperatures during the solidification of Inconel 738, dampens contraction stresses caused by solidification, and prevents the formation of hot cracks.

Statements & Declarations
Funding
No funding was received for conducting this study. However, the authors received equipment support from Iran Laser Industrial Research Center (Laser Hub) for conducting laser welding and laser cladding experiments.

Competing Interests

The authors have no relevant financial or non-financial interests to disclose.

Author Contributions

All authors contributed to this study. Design of experiments, material preparation, data collection and analysis were made by *Peyman Toosi*. Study conceptualization, manuscript review & editing, and project supervision were performed by *Hami Zarepour*. Data analysis & curation as well as results validation were made by *Mohammad-Ali Rezaei*.

References

[1] Salwan GK, Subbarao R, Mondal S (2021) Comparison and selection of suitable materials applicable for gas turbine blades. Mater Today Proc 46:8864–8870. https://doi.org/10.1016/j.matpr.2021.05.003

[2] Liu R, Wang Z, Sparks T, Liou F, Newkirk J (2017) Aerospace applications of laser additive manufacturing. In: Brandt M (ed) Laser Additive Manufacturing. Woodhead Publishing Elsevier, pp. 351–371. https://doi.org/10.1016/B978-0-08-100433-3.00013-0.

[3] Kataria R, Singh RP, Sharma P, Phanden RK (2021) Welding of super alloys: A review. Mater Today Proc 38:265–268. https://doi.org/10.1016/j.matpr.2020.07.198

[4] AL-Nafeay RH, AL-Roubaiy AO, Omidvar H (2021) Overview of joining and repairing techniques of Ni-based superalloy for industrial gas turbine applications. IOP Conf Ser: Mater Sci Eng 1094:012141

[5] Carter TJ (2005) Common failures in gas turbine blades. Eng Fail Anal 12:237–247. https://doi.org/10.1016/j.engfailanal.2004.07.004

[6] Su CY, Chou CP, Wu BC, Lih WC (1997) Plasma transferred arc repair welding of the nickel-base superalloy IN-738LC. J Mater Eng Perform 6:619–627. https://doi.org/10.1007/s11665-997-0055-7

[7] Arjakine N, Bruck J, Gru¨ger B, Seeger DM, Wilkenhoener R (2008) Advanced weld repair of gas turbine hot section components. ASME Turbo Expo 2008: Power for Land, Sea, and Air (ASMEDC) 1: 559-564. https://doi.org/10.1115/GT2008-51534

[8] Xu H, Huang H, Liu Z (2021) Influence of plasma transferred arc remelting on microstructure and properties of PTAW-deposited Ni-based overlay coating. J Therm Spray Tech 30:946–958. https://doi.org/10.1007/S11666-021-01183-1

[9] Banerjee K, Richards NL, Chaturvedi MC (2005) Effect of filler alloys on heat-affected zone cracking in preweld heat-treated IN-738 LC gas-tungsten-arc welds. Metall Mater Trans A 36:1881–1890. https://doi.org/10.1007/s11661-005-0051-1

[10] Durocher J, Richards NL (2007) Characterization of the micro-welding process for repair of nickel base superalloys. J Mater Eng Perform 16:710–719. https://doi.org/10.1007/s11665-007-9112-5

[11] Keivanloo A, Naffakh-Moosavy H, Miresmaeili R (2021) The effect of pulsed laser welding on hot cracking susceptible region size and weld pool internal geometry of Inconel 718: Numerical and experimental approaches. CIRP J Manuf Sci Technol 35:787–794. https://doi.org/10.1016/j.cirpj.2021.09.001

[12] Lippold JC, Kiser SD, DuPont JN (2011) Welding metallurgy and weldability of nickel-base alloys. John Wiley & Sons, Hoboken, New Jersey

[13] Zhong M, Liu W (2010) Laser surface cladding: the state of the art and challenges. Proc Inst Mech Eng, Part C: J Mech Eng Sci 224:1041–1060.

https://doi.org/10.1243/09544062JMES17
[14] Bielenin M, Bergmann JP, Sieber P (2017) Repair of nickel-based superalloys by pulsed Nd:YAG welding with wire feeding. Proc Lasers in Manuf Conf (LiM 2017) München, Germany
[15] Brandt M, Sun S, Alam N, Bendeich P, Bishop A (2009) Laser cladding repair of turbine blades in power plants: from research to commercialisation. Int Heat Treat Surf Eng 3:105–14. https://doi.org/10.1179/174951409X12542264513843
[16] Chen C, Wu HC, Chiang MF. Laser cladding in repair of IN738 turbine blades (2008) Int Heat Treat Surf Eng 2:140–6. https://doi.org/10.1179/174951508X446484
[17] Taheri M, Halvaee A, Kashani-Bozorg SF (2019) Effect of Nd:YAG pulsed-laser welding parameters on microstructure and mechanical properties of GTD-111 superalloy joint. Mater Res Express 6:076549. https://doi.org/10.1088/2053-1591/ab1534
[18] Kou S (2003) Welding metallurgy, 3rd edn. John Wiley & Sons, Hoboken, New Jersey
[19] Cherif S, Zakaria B (2018) Effect of welding current on microstructures and mechanical properties of welded Ni-base superalloy INC738LC. World J Eng 15:14–20. https://doi.org/10.1108/WJE-03-2017-0064/FULL/XML
[20] Taheri M, Halvaee A, Golezani AS, Kashi AA (2020) Investigation of melting rate in welding of IN738 Nickel-based superalloy by Nd:YAG pulsed-laser method. Eng Res Express 2:045025. https://doi.org/10.1088/2631-8695/abcd0d.
[21] Rezaei MA, Naffakh-Moosavy H (2018) The effect of pre-cold treatment on microstructure, weldability and mechanical properties in laser welding of superalloys. J Manuf Process 34:339–48. https://doi.org/10.1016/j.jmapro.2018.06.018
[22] Taheri M, Kashani-Bozorg SF, Alizadeh A, Beni MH, Jam JE, Khorram A (2021) Analysis of liquation and solidification cracks in the electron beam welding of GTD-111 nickel-base superalloy joint. Mater Res Express 8: 076507. https://doi.org/10.1088/2053-1591/ac1007
[23] Han S-W, Cho W-I, Na S-J, Kim C-H (2013) Influence of driving forces on weld pool dynamics in GTA and laser welding. Weld World 57:257–264. https://doi.org/10.1007/s40194-012-0020-4